A Machine-Learning-Based Interturn Short-Circuit Diagnosis for Multi-Three-Phase Brushless Motors

(Article begins on next page)

28 April 2024

This is the final peer-reviewed accepted manuscript of:

Terms of use:

A Machine Learning-Based Inter-Turn Short-Circuit Diagnosis for Multi-Three-Phase Brushless Motors

Antonio Femia, Giacomo Sala, *Member, IEEE*, Luca Vancini, Gabriele Rizzoli, Michele Mengoni, *Member, IEEE* Luca Zarri, *Senior Member, IEEE*, and Angelo Tani

Abstract—Over the past few years, Artificial Intelligence (AI) techniques have become one of the most exciting technologies of our age. This fascinating field paves the way for new possibilities and extends to almost all areas of industry and research. This paper illustrates a Short-Circuit (SC) diagnosis strategy for a multi-three-phase brushless AC motor drive based on Machine Learning (ML). A thorough model of the electrical machine is obtained through specific finite-element simulations and used to replicate various fault scenarios. This model quickly yields a large amount of data, which is then employed for training the ML algorithms. Once trained, the ML models are tested, with experimental data directly obtained from a prototype of multiphase drive, to verify the effectiveness of the diagnostic algorithms. The ML algorithms allow monitoring the health condition of the machine, distinguishing and localizing two types of faults, i.e., inter-turn SCs and Extra Turns (ETs), placed in different coils of the machine.

Index Terms—Artificial intelligence, circuit fault, fault diagnosis, fault location, machine learning, multiphase drives, neural network.

I. INTRODUCTION

INTEREST in multiphase motors has significantly grown in recent years due to a general increase in reliability requirements for industrial drives in various applications [1]–[3]. It has been proven that a multiphase drive can often continue to operate under fault conditions, albeit at reduced performance.

The advantages of multiphase drives, such as the fault tolerance capability, combined with those of synchronous machines, such as high efficiency, high power density, and excellent dynamic performance, make multiphase synchronous machines a promising technology.

Among the multiphase layouts, the multi-three-phase one offers advantages in terms of simplicity and modularity of the converter architecture, which is based on conventional three-phase inverters.

The advancements in multiphase drives require increasingly sophisticated control and diagnostic techniques to satisfy the reliability and performance requirements. In this regard, Artificial Intelligence (AI) methods provide an excellent answer to these problems [4].

Antonio Femia, Giacomo Sala, Luca Vancini, Gabriele Rizzoli, Michele Mengoni, Luca Zarri, and Angelo Tani are with the Department of Electrical, Electronic, and Information Engineering "Guglielmo Marconi", University of Bologna, Italy (email: antonio.femia3@unibo.it, g.sala@unibo.it, luca.vancini4@unibo.it, gabriele.rizzoli@unibo.it, michele.mengoni@unibo.it, luca.zarri2@unibo.it, angelo.tani@unibo.it).

The analytical approach to fault diagnosis often requires radical assumptions. It is necessary to know how the input data and the results are related [5]. This requirement is overcome by ML, in which the algorithm itself understands the relationship between input and output data. This technology can be advantageous in fault diagnosis, where determining the analytical expressions describing a fault is often challenging.

Moreover, different faults can impact the electric drive with similar effects. For instance, asymmetries in the windings, such as resistance and inductance imbalances, or even an unequal number of turns in the phases due to defects in the manufacturing process, can exhibit effects similar to those of an inter-turn short circuit. Whereas an SC could lead to the failure of the drive, the effect of an ET in a phase is almost negligible.

Inter-turn SCs have a prominent role in the critical faults of electrical machines since they generate large uncontrolled circulating currents which produce torque ripples and vibrations and can quickly lead to high temperatures. Consequently, diagnosing intern-turn SC faults is essential to prevent catastrophic failures [6]. Fig. 1 shows a schematic view of an inter-turn SC. The magnitude of the short-circuit circulating current i_{sc} depends on the number of short-circuited turns, their position in the slot, the speed of the machine, and the electromagnetic coupling among the various sub-windings.

Finally, it is worth identifying the phase in which a fault occurs for prompt intervention and to help repair the machine once it has been powered off. The fault localization is particularly useful in multi-three-phase drives, where the motor has
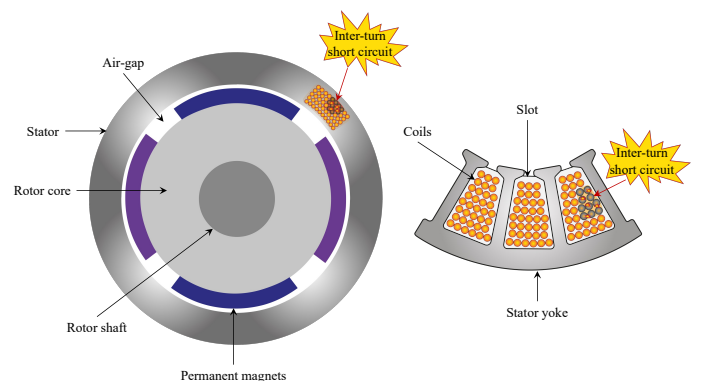

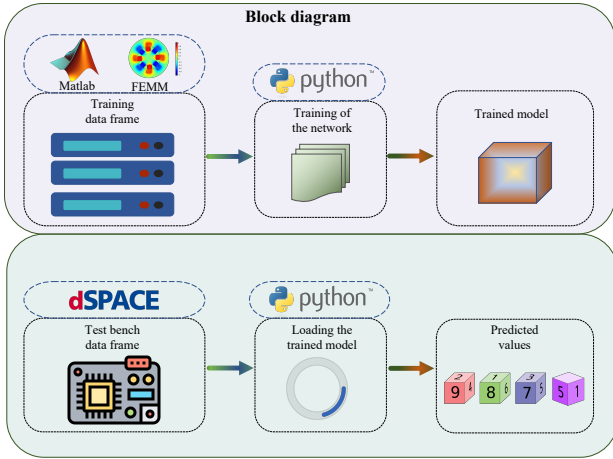Fig. 1. View of a short-circuit affecting 10 turns of the stator winding.

Fig. 2. Scheme of the proposed fault diagnosis strategy.

different sets of three-phase distributed windings, and the one in which the fault takes place can be disconnected to preserve the integrity and partial functionality of the drive, depending on the type of fault.

To ensure service continuity, it is necessary to implement a post-fault control strategy. Recently, several strategies have been proposed for a wide variety of faults, such as rotor faults [7], broken bars in induction motors [8], [9], and inverter faults [10]–[12]. Many of these have been developed using an AI approach [12]–[15], which proves the flexibility of this technology.

If an SC occurs, disconnecting the faulty phase does not prevent the short-circuit current from circulating. However, this current is an increasing function of the motor speed and has the tendency to reach a constant value since the inductive behavior of the short-circuited turns dominates at high speeds. In some applications, such as electric propulsion, the reference motor speed could be reduced by the control system as soon as a fault is detected. The electric drive could still operate, even with low performance. Hence, locating the fault allows one to compensate for the resulting imbalance and keep the motor running.

The key contributions of this work include the theoretical derivation of a semi-analytical model for a six-phase permanent magnet synchronous motor (6PMSM) under fault conditions and the application of ML strategies for SC fault diagnosis:

1) an effective finite element-based model able to simulate several faults under different operating conditions in a short amount of time is presented;
2) the faults are investigated with different ML algorithms;
3) the fault location is obtained by the ML strategies, which identify the fault type and the faulty phase from the experimental data;
4) the employed ML models distinguish an SC fault from an ET fault and recognize when they occur together.

Section II illustrates the developed methodology, based on a model of a multi-three-phase motor used to train the ML algorithm, and identifies the most significant variables for the fault diagnosis. Section III comments on the performance of

the ML algorithm, and Section IV presents the experimental results carried out to validate the effectiveness of the developed diagnostic method.

II. DIAGNOSTIC METHODOLOGY

A methodology for diagnosing faults and asymmetries, whose workflow is shown in Fig. 2, is presented in the following. Section II.A illustrates a general approach for the machine model, valid in faulty conditions, and identifies the parameters that affect the short-circuit current. Section II.B introduces a space vector representation that decouples the variables related to different harmonics of the airgap magnetic field and allows choosing the output variables for the ML model. The diagnostic strategy requires identifying specific harmonics in the phase voltage setpoints to classify the machine fault. Since an ML model involves a training process, Section II.C explains how the training data is generated. The learning algorithm finds patterns in the training data that relate the attributes of the input data to the target (the machine healthy-faulty condition to be predicted) and outputs a machine-learning model that captures these patterns.

A. Machine Model and Equations

This Section introduces the fundamental phase voltage equations that describe the behavior of an electrical machine under healthy and faulty conditions, including a possible asymmetry in the stator winding. These equations are used in the following to identify relevant variables for the diagnostics and are solved to build a training dataset for the proposed algorithms. Although the techniques illustrated in this paper are valid for a generic multi-three-phase machine with m phases, the focus is on a specific case study for the sake of simplicity.

The electric motor considered in this Section is the prototype used for the experimental tests, which is a 6PMSM with two sets of three-phase distributed windings spatially shifted by 30 electrical degrees. The two windings are star connected and have an independent neutral point each. The machine has four poles with two slots per pole per phase, and the coil pitch is shortened by one slot. Overall, 48 coils of 10 turns in series are distributed in 48 slots (8 coils in series per phase) and arranged as illustrated in Fig. 3, where phases 1, 2, 3, 4, 5, and 6 are respectively referred to as A_1, B_1, A_2, B_2, A_3, and B_3. Fig. 4 shows the 6PMSM electric circuit. The lumped parameters R_k and L_{kk} refer to the phase resistance and self-inductance of the kth winding, while e_k is the electromotive force induced in the same winding by the rotor magnets. The mutual inductances $L_{z,k}$ between phases k and z are not illustrated to make the figure simpler but are considered in the equations.

In general, to model winding asymmetries such as an ET and imbalances, these parameters must differ for all the phases. Furthermore, in case of an SC fault, an additional parallel ohmic branch R_{sc} appears in the electric circuit for the faulty phase (A_3 in Fig. 4). Also, the short circuit halves the faulty phase. The phase current flows in the healthy portion, while the SC current adds up to the phase current in the short-circuited portion. The resistance R_{sc} in the SC branch is included to
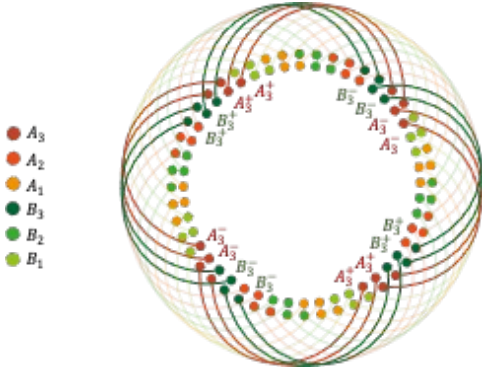
Fig. 3. Stator winding layout of the proposed 6PMSM. The phases A_3 and B_3 are highlighted.

Fig. 4. Circuital model of an SC inserted in the phase A_3.

consider a non-ideal short circuit (this parameter can also be set to zero). In a motor without SC faults, the voltage equation for the xth phase can be written as follows:

$$v_x = R_x i_x + \sum_{z=1}^{m} L_{z,x} \frac{di_z}{dt} + e_x \tag{1}$$

In case of a short circuit in the yth phase ($A3$ in Fig. 4), the resulting set of equations is composed of the equations of the healthy phases ($x = 1, 2, ..., m$ and $x \neq y$), an equation (whose quantities are denoted by the superscript $'$) for the healthy portion of the yth phase, and an equation (whose quantities are denoted by the superscript $*$) for the short-circuited portion y^* of the same phase y:

$$
\begin{aligned}
v_x &= R_x i_x + \sum_{\substack{z=1 \\ z \neq y}}^{m} L_{zx} \frac{di_z}{dt} + L_{y'x} \frac{di_y}{dt} + L_{y^*x} \frac{di_{y^*}}{dt} + e_x \\
v_{y'} &= R_{y'} i_y + \sum_{\substack{z=1 \\ z \neq y}}^{m} L_{zy'} \frac{di_z}{dt} + L_{y'y'} \frac{di_y}{dt} + L_{y^*y'} \frac{di_{y^*}}{dt} + e_{y'} \\
v_{y^*} &= -R_{sc} i_{sc} = \\
&= R_{y^*} i_{y^*} + \sum_{\substack{z=1 \\ z \neq y}}^{m} L_{zy^*} \frac{di_z}{dt} + L_{y^*y^*} \frac{di_{y^*}}{dt} + L_{y'y^*} \frac{di_y}{dt} + e_{y^*}
\end{aligned}
\tag{2}
$$

where i_{y^*} is the current flowing through the short-circuited portion of the faulty phase, and v_y is the phase voltage at the terminals of the phase y:

$$i_{y^*} = i_y + i_{sc}, \quad v_y = v_{y'} + v_{y^*}. \tag{3}$$

Equations (1)-(3) are general for any permanent magnet motor with an isotropic rotor and negligible saturation of the magnetic circuits. They can be used to perform both transient and steady-state simulations of a multiphase drive while considering the possibility of asymmetries or faults. Hereafter, only steady-state operations are considered to quickly identify a large dataset containing sufficient information about the state of the motor in many working conditions and fault scenarios. Also, it is assumed that the control system of the motor is ideal, and it can maintain the waveform of the phase currents sinusoidal even in case of a fault. Under these assumptions, each variable of the electric drive can be expressed as a time
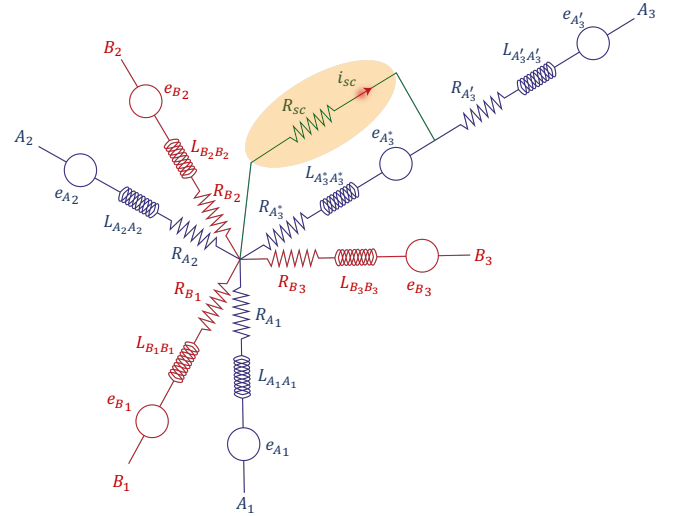
Fourier series. In particular, the electromotive forces, voltages, and currents of the kth phase can be written as follows:

$$
\begin{aligned}
e_k &= \sum_{h=1}^{\infty} \Re\{\overline{E}_{kh}\, e^{jh\omega t}\}, \quad v_k = \sum_{h=1}^{\infty} \Re\{\overline{V}_{kh}\, e^{jh\omega t}\}, \\
i_k &= \Re\{\overline{I}_k\, e^{j\omega t}\}, \quad i_{sc} = \sum_{h=1}^{\infty} \Re\{\overline{I}_{sc,h}\, e^{jh\omega t}\}
\end{aligned}
\tag{4}
$$

where j is the imaginary unit, h is the harmonic order, and ω is the electrical angular speed of the motor. The term representing the rotor electromotive force, $\overline{E}_{kh} = jh\omega\overline{\phi}_{kh}$, is proportional to the phasor $\overline{\phi}_{kh}$ of the hth harmonic of the flux linkage due to the magnets through the kth phase.

It is possible to separately consider the effects associated with the fundamental spatial harmonic of the magnet flux distribution at the airgap ($h = 1$) and those related to the higher-order harmonics. By substituting (4) in (2), assuming $L_{y'x} + L_{y^*x} = L_{yx}$, and considering (3), the set of output voltage equations for the fundamental component ($h = 1$) becomes:

$$\overline{V}_{x1} = R_x \overline{I}_x + j\omega\left[\sum_{z=1}^{m} L_{zx}\overline{I}_z + L_{y^*x}\overline{I}_{sc1} + \overline{\phi}_{x1}\right] \tag{5}$$

$$
\begin{aligned}
\overline{V}_{y1} &= \overline{V}_{y^*1} + \overline{V}_{y'1} = -R_{sc}\overline{I}_{sc1} + R_{y'}\overline{I}_y + \\
&\quad + j\omega\left[\sum_{z=1}^{m} L_{zy'}\overline{I}_z + L_{y^*y'}\overline{I}_{sc1} + \overline{\phi}_{y'1}\right].
\end{aligned}
\tag{6}
$$

Considering the identity $L_{y^*y^*} + L_{y'y^*} = L_{yy^*}$, $\overline{I}_{sc1}$ becomes as follows:

$$\overline{I}_{sc1} = -\frac{R_{y^*}\overline{I}_y + j\omega\left[\sum_{z=1}^{m} L_{zy^*}\overline{I}_z + \overline{\phi}_{y^*1}\right]}{R_{sc} + R_{y^*} + j\omega L_{y^*y^*}}. \tag{7}$$

Equation (7) shows that the fundamental time harmonic of the SC current is a function of the phasor $\overline{\phi}_{y^*1}$ of the fundamental flux linkage due to the magnets through the short-circuited portion of the yth phase, the rotor speed, and the phasors of the phase currents $\overline{I}_z$ ($z = 1, 2, ..., m$). The electromotive force induced in the short-circuited turns rises
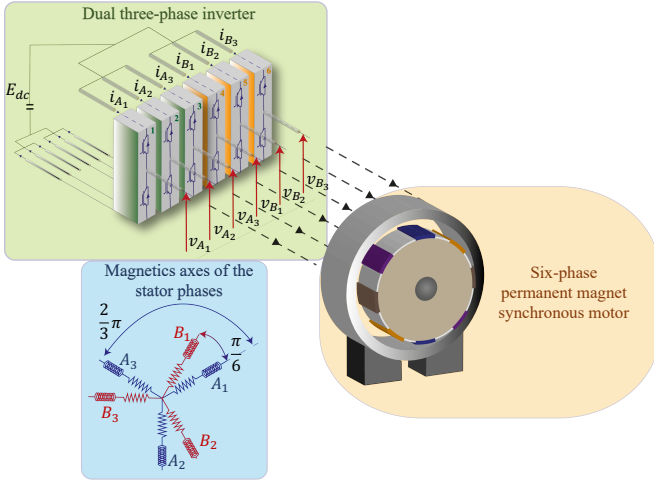
Fig. 5. Layout of the proposed 6PMSM drive.

as the motor speed increases, but the circulating current tends to a constant value since the reactive part of the impedance prevails on the resistive part.

Equations (5) and (6) show that the resulting phase voltage for the healthy and faulty phases depends on the same quantities through $\overline{I}_{sc1}$. The higher-order time-harmonic contributions can be calculated in a similar manner. The following set of equations can be written for the hth time harmonic:

$$\overline{V}_{xh} = jh\omega[L_{y^*x}\overline{I}_{sc,h} + \overline{\phi}_{xh}] \tag{8}$$

$$\overline{V}_{yh} = -R_{sc}\overline{I}_{sc,h} + jh\omega[L_{y^*y'}\overline{I}_{sc,h} + \overline{\phi}_{y'h}] \tag{9}$$

$$\overline{I}_{sc,h} = -\frac{jh\omega\overline{\phi}_{y^*h}}{R_{sc} + R_{y^*} + jh\omega L_{y^*y^*}}. \tag{10}$$

It is worth observing that, for a given set of motor parameters and speeds, (8)-(10) are functions of the motor asymmetry and fault condition. This result can be used to develop fault diagnosis strategies for multiphase drives, where the harmonic contributions of the motor variables (currents, voltages, etc.) can be mapped in different vector spaces, as described in Section II-B.

B. Space Vector Representation for Training Dataset

This Section illustrates an approach to the modeling of multiphase drives. It focuses on the particular case of the 6PMSM under study but can be easily extended to other multiphase layouts.

The considered 6PMSM is fed by a two-level dual three-phase voltage source converter, as shown in Fig. 5. The converter is connected to a single dc-link providing $2^6 = 64$ possible switching states [16]. The two three-phase sub-windings are star-connected to two independent neutral points.

Through the Vector Space Decomposition (VSD) approach, the six quantities of the dual three-phase motor can be fully represented in terms of space vectors, which can be calculated by applying an extended Clarke transformation. The space vectors $\overline{v}_{A\rho}$ and $\overline{v}_{B\rho}$ of the phase voltages of windings A and B are defined for $\rho = 0, 1, ..., \infty$ as follows:

$$\overline{v}_{A\rho} = \tfrac{2}{3}[v_{A_1} + v_{A_2}\overline{\alpha}^\rho + v_{A_3}\overline{\alpha}^{2\rho}]$$
$$\overline{v}_{B\rho} = \tfrac{2}{3}[v_{B_1} + v_{B_2}\overline{\alpha}^\rho + v_{B_3}\overline{\alpha}^{2\rho}] \tag{11}$$

where $\overline{\alpha}$ is a unit vector equal to $e^{j\frac{2}{3}\pi}$, representing the electrical phase shift between the magnetic axes of the phases in the same three-phase winding. When ρ is a multiple of 3, $\overline{v}_{A\rho}$ and $\overline{v}_{B\rho}$ are usually referred to as zero-sequence components v_{A0} and v_{B0} of the phase voltages.

Vectors $\overline{v}_{A\rho}$ and $\overline{v}_{B\rho}$ are used to define the voltage space vectors of the multiphase machine as follows:

$$\overline{v}_\rho = \tfrac{1}{2}\overline{v}_{A\rho} + \tfrac{1}{2}\overline{v}_{B\rho}\overline{\beta}^\rho \tag{12}$$

where $\overline{\beta}$ is a unit vector equal to $e^{j\frac{\pi}{6}}$, representing the electrical angular shift between the two three-phase windings. The following equations can be demonstrated:

$$\overline{v}_{12k+\rho} = \overline{v}_\rho$$
$$\overline{v}_{12k-\rho} = \overline{v}_\rho^* \tag{13}$$

where k is any real integer number. As a general result, only the space vectors with $\rho = 1$, 3, and 5 are independent and sufficient to unequivocally represent the set of variables $v_{A_1}, v_{A_2}, v_{A_3}, v_{B_1}, v_{B_2}$, and v_{B_3}.

Equations (11) and (12) can be applied to the other machine quantities, such as currents and fluxes. However, space vector $\overline{i}_3$, calculated by applying (12) to the phase currents, is associated with the zero-sequence component of the currents, which is zero due to the star connection of windings A and B ($\overline{i}_3 = i_{A0} + ji_{B0} = 0$). Consequently, only voltage vectors $\overline{v}_1$ and $\overline{v}_5$ must be used to control the current vectors $\overline{i}_1$ and $\overline{i}_5$. In particular, space vector $\overline{i}_1$ is controlled to produce the desired torque and flux, while space vector $\overline{i}_5$ is kept equal to zero.

At steady-state operating conditions, when the motor rotates at constant angular speed ω, the current space vectors are:

$$\overline{i}_1 = \overline{i}_{ref}e^{j\omega t}$$
$$\overline{i}_5 = 0. \tag{14}$$

For a healthy motor, without asymmetries, the voltage and flux vectors ($\rho = 1, 5$) can be expressed as complex Fourier series as follows:

$$\overline{v}_\rho = \sum_{h=1}^{\infty}\overline{v}_\rho^{h+}e^{jh\omega t} + \sum_{h=1}^{\infty}\overline{v}_\rho^{h-}e^{-jh\omega t}$$
$$\overline{\varphi}_\rho = \sum_{h=1}^{\infty}\overline{\varphi}_\rho^{h+}e^{jh\omega t} + \sum_{h=1}^{\infty}\overline{\varphi}_\rho^{h-}e^{-jh\omega t} \tag{15}$$

where the notation $h+$ and $h-$ is used to identify the hth harmonic component of the positive and negative sequences, respectively.

The stator voltage equation of the healthy machine can be written in terms of space vectors as follows:

$$\overline{v}_\rho = R_s\overline{i}_\rho + \frac{d\overline{\varphi}_\rho}{dt}. \tag{16}$$

If (14) and (15) are combined with (16), the balance of the fundamental harmonic (1+) for $\rho = 1$ yields:

$$\overline{v}_1^{1+} = R_s\overline{i}_{ref} + j\omega\overline{\varphi}_1^{1+} \tag{17}$$

Direct sequence harmonic components $\overline{v}_5^{h+}$

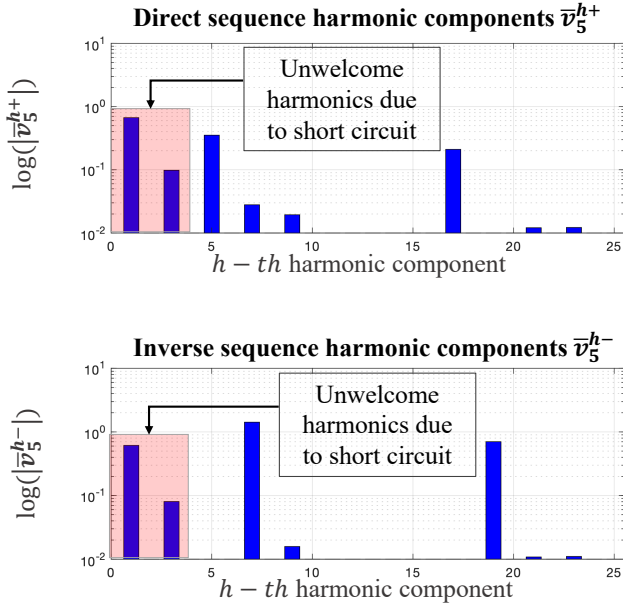## Inverse sequence harmonic components $\overline{v}_5^{h-}$

Fig. 6. Time-harmonic contributions to the space vector $\overline{v}_5$. The significant terms that appear in $\overline{v}_{5,DS}$ due to a short circuit fault are highlighted.

while the other harmonic components are as follows:

$$
\begin{aligned}
\overline{v}_1^{h+} &= jh\omega\overline{\varphi}_1^{h+} \\
\overline{v}_1^{h-} &= -jh\omega\overline{\varphi}_1^{h-} \\
\overline{v}_5^{h+} &= jh\omega\overline{\varphi}_5^{h+} \\
\overline{v}_5^{h-} &= -jh\omega\overline{\varphi}_5^{h-}.
\end{aligned}
\tag{18}
$$

In contrast, additional voltage contributions are required to keep the current waveform sinusoidal if a fault occurs or an asymmetry is present. In the case of asymmetrical windings, the main additional voltage contributions are expected to affect the positive and negative sequences at the fundamental frequency ($\overline{v}_1^{1+}$, $\overline{v}_1^{1-}$, $\overline{v}_5^{1+}$, $\overline{v}_5^{1-}$). Instead, in case of an extra turn in a phase or a short-circuit fault, the unbalanced electromotive forces produced by the rotor magnets cause time harmonics with an order higher than 1. The most important ones are often at three times the fundamental frequency ($\overline{v}_1^{3+}$, $\overline{v}_1^{3-}$, $\overline{v}_5^{3+}$, $\overline{v}_5^{3-}$). Furthermore, since an SC current produces a pulsating airgap flux and, consequently, a torque ripple, the speed regulator is expected to partially compensate for this unexpected torque disturbance by generating distortion in both the current vector $\bar{i}_1$ and the voltage vector $\overline{v}_1$, while $\overline{v}_5$ is controlled to keep the current $\bar{i}_5$ at zero.

A change in $\overline{v}_5$ is a necessary but not sufficient condition to detect the presence of a fault. To diagnose the fault, the $\overline{v}_5$ harmonic components of order -1, +1, -3, and +3 are monitored. The other harmonics of $\overline{v}_5$ are not used as diagnostic indices due to their lower magnitudes and because they are mainly caused by magnet-induced back-emf harmonics and slotting effects.

Fig. 6 illustrates the harmonics that arise in $\overline{v}_5$ in case of a particular short-circuit fault.

Therefore, it seems reasonable to develop a Diagnosis Strategy (DS) focusing on the 1st and 3rd time harmonic

TABLE I
MOTOR PARAMETERS

Motor data	Values	Units
Rated speed	1500	RPM
Rated torque	25	Nm
Pole pairs, p	2	-
Fundamental harmonic of the magnets flux	0.393	Wb
Magnetic airgap thickness (including magnets)	7	mm
Magnet thickness	5	mm
Number of slots	48	-
Conductors per slot	20	-
Phase resistance, R_s	0.36	Ω
Inductance of the first Clark space, L_1	0.0056	H
Inductance of the fifth Clark space, L_5	0.00081	H
Axial active length	70	mm
Stator inner radius	75	mm

components of $\overline{v}_5$:

$$
\overline{v}_{5,DS} = \overline{v}_5^{1+}e^{j\omega t} + \overline{v}_5^{1-}e^{-j\omega t} + \overline{v}_5^{3+}e^{j3\omega t} + \overline{v}_5^{3-}e^{-j3\omega t}. \tag{19}
$$

The contributions to the diagnostic space vector $\overline{v}_{5,DS}$ in (19) are zero in the case of a healthy machine with sinusoidal back-emfs due to the rotor magnets, according to (18). In contrast, the components $\overline{v}_5^{1+}$ and $\overline{v}_5^{1-}$ are expected in case of asymmetries in the phase inductances and resistances. Finally, $\overline{v}_5^{3+}$ and $\overline{v}_5^{3-}$ arise from an unequal number of turns in the phases (ET), or a short-circuit (SC).

These four complex vector contributions represent the diagnostic variables used to train the ML algorithms described in Section III.

C. Finite Element-Based Parameter Extrapolation

Several machine parameters, such as the self and mutual inductances, are required to evaluate the expected values of the diagnostic variables in (19). Motor suppliers do not provide enough parameters to calculate these values, especially in case of asymmetries and faults. Hence, analytical or numerical models must be developed to calculate them. In this paper, an approach based on finite-element analysis is presented. The motor turns are considered independent circuits. Each turn is characterized by resistance, self-inductance, mutual inductance with all the other turns, and flux linkage of the magnet field. Lastly, the inductances and resistances of each phase in (8) and (9) are calculated according to the parallel/series connections of the turns that constitute each sub-winding, and the short circuit resistance R_{sc} is simply added as an extra motor parameter.

The considered 6PMSM motor, whose main parameters are listed in Tab. I, has 8 coils per phase in a dual layer layout with 11 turns per coil (10 turns plus 1 possible ET), which corresponds to a total of 528 turns simulated in the finite-element model. A 528x528 inductance matrix is built. Then, the flux linkage due to the excitation field through the 528 turns must be calculated for each rotor position.

Calculating the flux linkage of each turn for every rotor position is time-consuming and can cause a significant computational effort. However, the flux linkage of a single turn can be easily calculated for every angular position of the rotor. Then, the spatial periodicity of the slots, as shown in Fig.
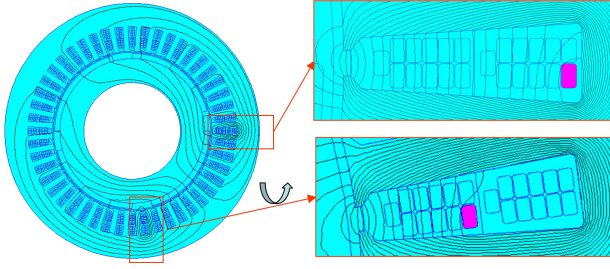
Fig. 7. Finite-element result: flux density distribution when a turn (i.e., 2 slot conductors) is supplied with current, and the magnets are fully demagnetized.

3, allows one to evaluate the flux linkage of the other turns without additional calculations. The flux linkage of a turn as a function of the rotor position is equal for all turns except for a phase shift, which depends on the position of the slots where the considered turns are placed.

Fig. 7 shows the flux density distribution when the current flows in only one turn. This numerical approach has been chosen to increase the accuracy in the definition of the dataset used to train the ML models.

A dataset of the selected outputs ($\overline{v}_5^{1+}$, $\overline{v}_5^{1-}$, $\overline{v}_5^{3+}$ and $\overline{v}_5^{3-}$) for various conditions, including asymmetries and faults, for different values of i_d, i_q, and speed can be quickly evaluated by using the model presented in II-A. The contributions to the voltage vector $\overline{v}_{5,DS}$ are calculated as presented in II-B.

The proposed approach can generate a dataset with the outputs of about one million asymmetries, faults, and operating scenarios in about 1.5 hours of numerical simulation in Matlab software and an AMD Ryzen 9 5900X Desktop Processor (12 CPU Cores, 3.7 GHz base clock frequency, 64 Gb RAM, NVIDIA QUADRO PNY P2000 Graphic Card). This computational time is low enough to consider this methodology as a valid solution for this research activity, and it can be easily adapted to motors with a different number of phases and other winding layouts.

III. MACHINE LEARNING MODELS

To test the effectiveness of the proposed diagnostic strategy, five ML models (Fig. 8) have been implemented [17]:

1) The Support Vector Machine (SVM) model aims to find a hyperplane in an N-dimensional space (N is the number of features) able to separate data points so that they can be correctly classified;
2) The K-Nearest Neighbors (KNN) model classifies each data point according to the similarity with those previously stored;
3) The Multilayer Perceptron (MPL) model is a feedforward algorithm including input and output layers, and one or more hidden layers with many neurons stacked together. Therefore, it is a "deep method", and its classification ability is based on the back-propagation mechanism;
4) The eXtreme Gradient Boosting (XGBoost) model is a decision-tree-based algorithm, which applies the principle of "boosting weak learners", using the gradient descent architecture to carry out the classification task;

5) The Gaussian Naive Bayes (GNB) model uses the Bayes theorem for the classification, assuming that each class follows a Gaussian distribution and the independence of the features.

Before starting the training task, the dataset was preprocessed to reduce its dimensionality. This is a common approach in Machine Learning as it allows a smaller dataset size to be used without losing the information needed for classification. Since the data are not separable in a linear way, Kernel Principal Component Analysis (KernelPCA) is used for dimensionality reduction. KernelPCA employs a spectral decomposition to determine the directions (eigenvectors) of the maximum variance, i.e., the directions where more information about the data frame is contained. This allows obtaining a smaller set of "artificial" orthogonal variables, starting from a set of correlated numerical variables, without losing information. Moreover, the variables are normalized in advance to prevent their variability from affecting the results of the KernelPCA. Fig. 9 displays the variance of the variables in the data frame along the new orthogonal directions. This result shows that eight directions (eigenvectors) are sufficient to describe 100% of the total data frame variance. Obviously, for a graphical representation, just three directions are needed. Fig.10 shows the samples of the training data frame in a space with lower dimensionality defined by the first three principal components. Although these three directions account for just 60% of the total variance, it is worth noting that some of the attributes are separable in the 3D space. For example, samples reflecting ET in different phases are distinctly represented by separable lines. This makes it easier for Machine Learning algorithms to perform the classification task. Once pre-processed, the data frame is used for training (Fig. 11).

Another essential aspect of an ML model concerns the hyperparameters, which directly control the learning process and determine the values of the model parameters that a learning algorithm ends up learning. The hyperparameters of each ML model are optimized with the Grid-Search technique in order to customize the models for the training task. The data frame used for the training task includes the following variables:

- **Targets**: labels for each class to be classified (Tab. II);
- $\boldsymbol{\omega}$: mechanical speed of the rotor;
- $\boldsymbol{i_d}$: $d-$axis current (directly correlated to the stator flux);
- $\boldsymbol{i_q}$: $q-$axis current (directly correlated to the torque);
- $\overline{\boldsymbol{v}}_{\boldsymbol{5,DS}}$: harmonics contributions, in magnitude and phase, due to SC and ET.
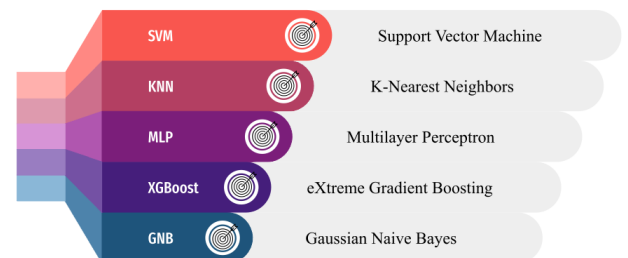
Fig. 8. Employed machine learning models.

Fig. 9. PCA results for the training data frame.
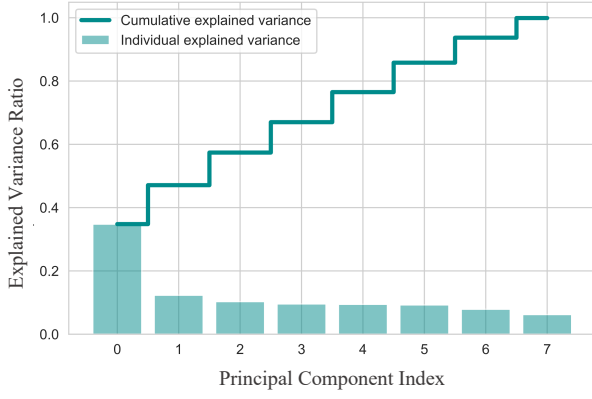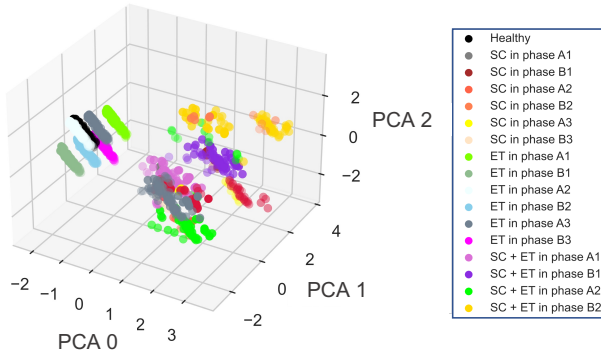
TABLE II
TARGETS EXPLANATION

Target	Short circuit (SC)	Extra turn (ET)
0	No	No
1	In phase A_1	No
2	In phase B_1	No
3	In phase A_2	No
...	...	...
7	No	In phase A_1
8	No	In phase B_1
...	...	...
13	In phase A_1	Yes (phase not predicted)
14	In phase B_1	No (phase not predicted)
...	...	...

Fig. 10. Samples of the training data frame mapped in a space defined by the first three principal components.

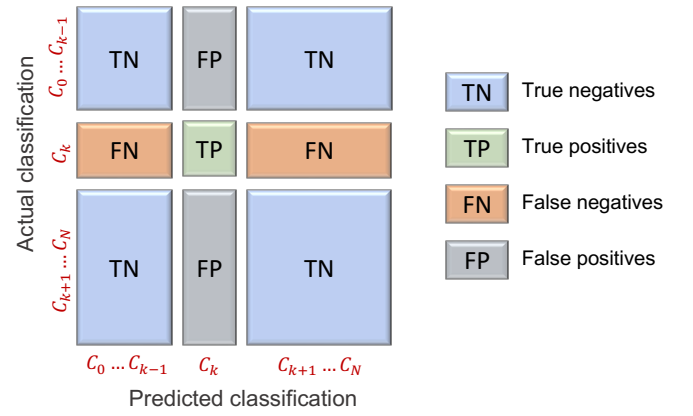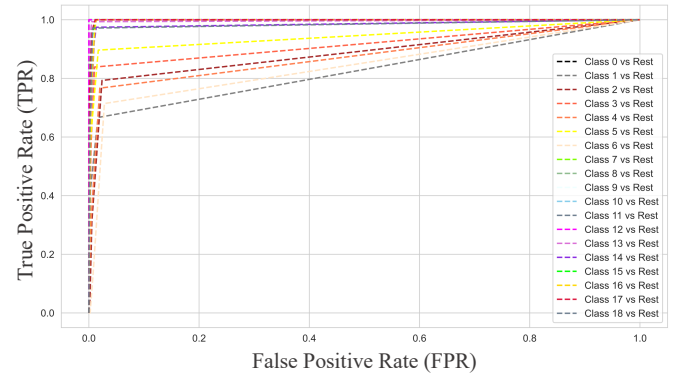Fig. 12. General confusion matrix for a multi-class model. The generic predicted class is labeled with C_k.

Fig. 11. Proposed training data frame as input to a general multilayer neural network structure.

Fig. 13. ROC (OvR strategy) curves obtained from the KNN model considering the test data.

IV. EXPERIMENTAL RESULTS

Considering the nomenclature for a general multi-class confusion matrix shown in Fig. 12, the performance of the ML models is evaluated through the following metrics (Tab. III):

- Training accuracy: accuracy of the model on actual data used for training (70% of the data frame obtained with Matlab/FEMM simulations);
- Test accuracy: accuracy of the model on data never used for training (30% of the data frame obtained with Matlab/FEMM simulations);
- Test bench accuracy: accuracy of the model on data directly obtained from the test bench acquisitions;
- k-fold accuracy: accuracy of the model on a limited set

of data obtained by dividing the overall Matlab/FEMM data frame into k non-overlapping folds. Each kth fold can be used as a retained test set, while all other bends are collectively used as a training dataset;
- Precision (PRE): the number of instances that are relevant, out of the total instances the model retrieved, calculated as $PRE = \frac{TP}{TP+FP}$;
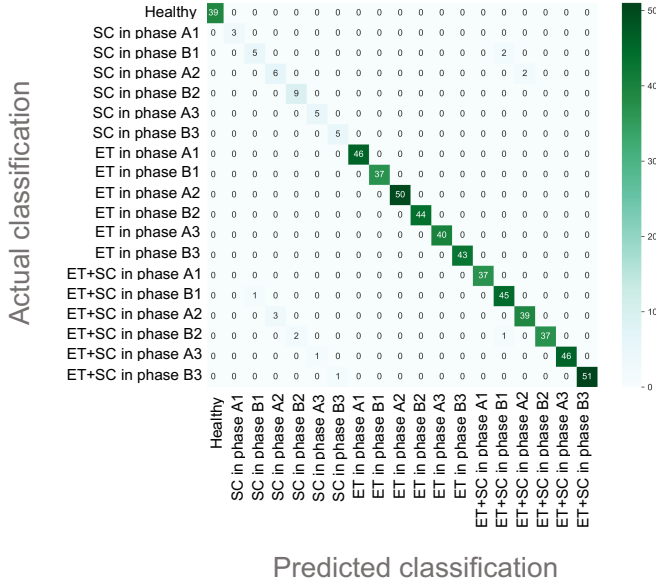- Recall (REC): the number of instances that the model

Fig. 14. Confusion matrix obtained from the test data frame with the SVM technique.

TABLE III
METRICS ADOPTED FOR EVALUATING THE ML MODELS

Model	Training accuracy	Test accuracy	Test bench accuracy	...
SVM	99.5%	97.3%	96.2%	...
KNN	96.6%	93.5%	93%	...
MLP	99.9%	95%	66.6%	
XGB	99.9%	95%	66%	
GNB	90.5%	88.1%	38.5%	
...	k-fold (k=5)	Precision	Recall	...
...	97 ± 2%	92.8%	95.2%	...
...	93 ± 1%	80.9%	78.9%	...
...	94 ± 1%	81.3%	82%	
...	94 ± 2%	90.9%	82.6%	
...	89 ± 2%	72.9%	74.1%	
...	AUC	F1-measure		
...	99.9%	93.7%		
...	78.9%	79.68%		
...	82%	80.7%		
...	82.6%	84.7%		
...	74.1%	72%		

correctly identified as relevant out of the total significant instances, calculated as $REC = \frac{TP}{TP+FN}$;

- AUC: the area under the Receiver Operator Characteristic (ROC), which are probability curves that plot the True Positive Rate (TPR) against the False Positive Rate (FPR), which are respectively defined as $TPR = \frac{TP}{FN+TP}$ and $FPR = \frac{FP}{FP+TN}$. AUC measures the ability of an ML model to distinguish among classes and is usually adopted for binary classification. AUC may be interpreted as the likelihood that a randomly chosen sample would be properly classified for various thresholds of the decision boundary. A model whose predictions are 100% wrong has an AUC equal to zero, whereas the AUC is one when the predictions are 100% correct.
- F1-score: it combines the precision and recall of a classifier into a single metric by taking their harmonic mean, calculated as $F1 = 2\frac{PRE \times REC}{PRE+REC}$.

Since the problem involves 19 classes, the last four metrics (PRE, REC, AUC, and F1-score) are determined using a "One vs Rest" (OvR) approach. It entails choosing one class and treating it as positive while treating the remaining ("the rest") as negative. This allows each class to be compared against all the others at the same time. For instance, Fig. 13 shows the ROC curves obtained with the OvR strategy considering the K-Nearest Neighbors (KNN) algorithm. OvR approach leads to consider the percentages in Tab. III as a macro average value.

Fig. 14 shows the confusion matrix resulting from the classification that the SVM model performs on the test data frame. As can be seen, almost all values are on the diagonal. This implies a match between predicted and actual values. Choosing the correct number of instances (rows of the data frame) for the training task is always an important matter. In fact, a wrong choice could lead to problems such as overfitting (too many parameters in the model and a high variability

of the classification) and underfitting (few parameters in the model and a high discrepancy in classification). In the first case, the model is too complex and sensitive to training data (high variance and low bias). In the second case, the model can accomplish a good classification since it has insufficient complexity (high bias and low variance). Thereby, the suspicion of overfitting arises when training accuracy and test accuracy curves are too far from each other. In contrast, when the models suffer from underfitting, both the mentioned curves drop rapidly to very low levels of accuracy.

A good ML model must reach a trade-off between variance and bias. Fig. 15 shows the accuracy curves and the optimal point representing the chosen number of instances of the training data frame for the Support Vector Machine (SVM) model. This approach allows one to find the optimal number of instances for each ML model, avoiding overfitting and underfitting.

The performance of the proposed AI-based fault detection strategies has been verified by experimental tests on the 6PMSM prototype shown in Fig. 16. The main motor parameters are listed in Tab. I.

A. Experimental Setup and Data Collection

The control system is implemented by using a dSPACE platform (MicroLabBox, DS1104), which manages the six-phase power converter through fiber-optic cables. The switching frequency of the converter is 8.8 kHz. An Elektro-Automatik power supply (EA-PS 9500 − 20) provides the drive DC link voltage, and a DC generator is employed as a mechanical load. Experimental tests are performed at reduced speed to avoid damaging the electric motor under test (e.g., overheating and
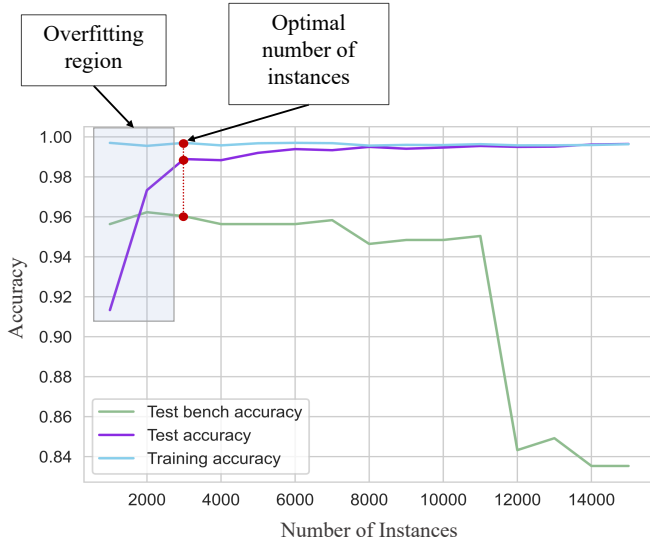
Fig. 15. Accuracies obtained from SVM model by varying the training data frame number of instances.

Fig. 16. Test bench.

Fig. 17. Experimental results in the case of a short circuit in phase B_3: currents $i_{A_1}, i_{B_1}, i_{A_2}, i_{B_2}, i_{sc}$ and diagnostic vectors $\overline{v}_5^{h+}$ (red) and $\overline{v}_5^{h-}$ (blue). The semi-analytical results are in dashed lines.

demagnetization). In particular, the maximum speed of the tests is set to about 700 r/min to maintain the short circuit current below 60 A.

A short circuit of 10 turns coincides with a short circuit of a coil. This means shorting 1/8 of the machine (12.5%). Conversely, 1 extra turn represents a variation of 1/81, that is 1,234%.

Fig. 17 shows a comparison between experimental and semi-analytical results when the motor features an SC of 10 turns in phase B3 and an ET in phase A3, while rotating at 700 rpm and controlled with a current i_{d1} of -5 A and a current i_{q1} of 2 A. The results show that the phase and short circuit currents have similar waveforms, whereas the diagnostic vectors ($\overline{v}_5^{1+}$, $\overline{v}_5^{1-}$, $\overline{v}_5^{3+}$ and $\overline{v}_5^{3-}$) match the predicted values less precisely but still represent the signature of the motor asymmetrical behavior. The mismatch between the simulation and experimental results is relatively small, and it is not simple to identify the primary cause. Some improvements may be expected if a more accurate system model is used. Also, the motor control algorithm cannot perfectly track the current references.

The SC resistance R_{sc} was updated to match the SC current with the measured value.

Three significant operating conditions are considered: no short circuit, a short circuit of 10 series turns in phase A_3 and a short circuit of 10 series turns in phase B_3. Furthermore, the motor has an ET in one coil (not affected by short circuit faults) of the phase A_3.

All the operating conditions mentioned above have been simulated to derive a wide experimental dataset (504 instances). Each instance is labeled with a target index, depicting the operating condition, according to the training data frame structure. Thus, the test bench data is employed to assess the effectiveness of the proposed strategy in correctly classifying the type of fault and its localization.
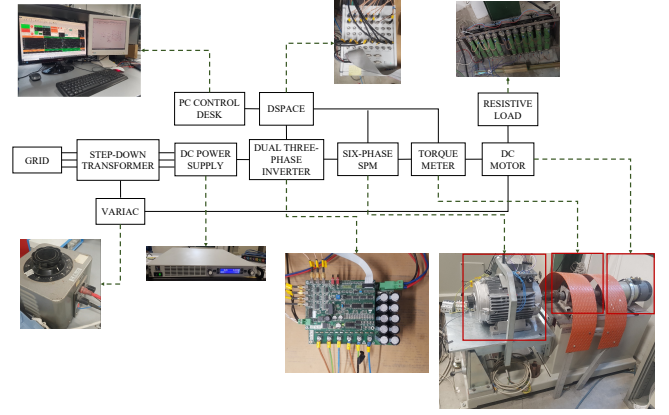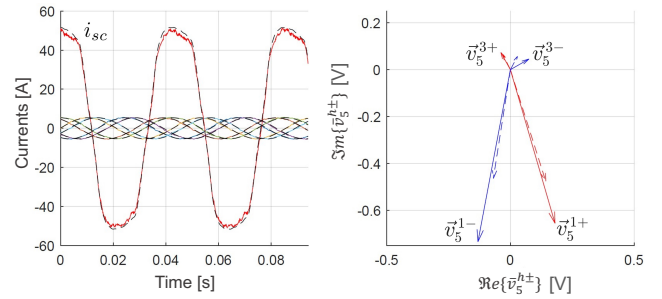
B. Localization and Classification of the Fault

Tab. III illustrates the results of each ML model implemented in this research work. This comparative study clearly shows that the best of the investigated techniques, in terms of metrics, is the SVM. It reaches an accuracy of 96.2% on the experimental data, which means that the ML algorithm can almost flawlessly predict the health state of the machine among all the 504 operating conditions. The KNN model exhibits good performance, although the precision and recall metrics differ by about 10% from the SVM. The MLP and XGB models show very similar performance and are both unable to reach high accuracy when assessed with the test bench data frame. Finally, GNB exhibits the poorest performance among all the metrics.

V. CONCLUSIONS

This paper presents a diagnostic method to detect and localize a short circuit fault in a 6PMSM using five machine-learning models. Moreover, the proposed strategy distinguishes a short circuit fault from an unbalance due to an additional turn.

Several techniques can be used to detect these faults, and machine learning does not automatically provide better diagnostic accuracy compared to existing methodologies since it depends on the type of machine learning model, its training, and the analyzed variables. However, artificial intelligence is promising because it may replace several specific tests or

techniques, usually performed at different stages and requiring different competence, with a single methodology. It is worth noting that an extra turn corresponds to a variation of 4 mΩ in the test machine (about 1% of the rated resistance), which is relatively small and comparable to the contact resistance of the terminals. Since the accuracy required to diagnose the extra turn must be better than 1%, the problem cannot be solved with a simple resistance test in industrial practice, and probably not even with the analysis of the electromotive forces of the machine.

The contribution of this paper is the development of machine learning algorithms to diagnose different types of faults, even occurring simultaneously. A semi-analytical model, based on a preliminary finite-element analysis to estimate the motor inductances, is developed. This model allows to obtain a large amount of data in a brief amount of time, corresponding to both healthy and faulty conditions for different operating points of the electric motor.

Once the data have been pre-processed and after choosing the correct number of instances to avoid overfitting and underfitting, 70% of the derived dataset is used for training purposes, while the remaining 30% is for testing. Thereby, the ML models are stored and tested with the experimental dataset.

Five ML algorithms were evaluated according to eight different metrics. Although they all showed high training and test accuracy, the SVM and KNN techniques performed significantly better. Specifically, the SVM was found as the best solution for correctly classifying these types of faults. The experimental validation demonstrates its effectiveness with an accuracy of 96.2%.

Further extension of the presented methodology is underway for other types of faults and motors.

REFERENCES

[1] F. Barrero and M. J. Duran, "Recent advances in the design, modeling, and control of multiphase machines—part i," *IEEE Transactions on Industrial Electronics*, vol. 63, no. 1, pp. 449–458, 2016.

[2] M. J. Duran and F. Barrero, "Recent advances in the design, modeling, and control of multiphase machines—part ii," *IEEE Transactions on Industrial Electronics*, vol. 63, no. 1, pp. 459–468, 2016.

[3] E. Levi, "Advances in converter control and innovative exploitation of additional degrees of freedom for multiphase machines," *IEEE Transactions on Industrial Electronics*, vol. 63, no. 1, pp. 433–448, 2016.

[4] S. Zhao, F. Blaabjerg, and H. Wang, "An overview of artificial intelligence applications for power electronics," *IEEE Transactions on Power Electronics*, vol. 36, no. 4, pp. 4633–4658, 2021.

[5] Y. L. Murphey, M. Masrur, Z. Chen, and B. Zhang, "Model-based fault diagnosis in electric drives using machine learning," *IEEE/ASME Transactions on Mechatronics*, vol. 11, no. 3, pp. 290–303, 2006.

[6] N. Yassa, M. Rachek, A. Djerdir, and M. Becherif, "Detecting of multi phase inter turn short circuit in the five permanent magnet synchronous motor," *International Journal of Emerging Electric Power Systems*, vol. 17, no. 5, pp. 583–595, 2016. [Online]. Available: https://doi.org/10.1515/ijeeps-2016-0084

[7] B. Kim, K. Lee, J. Yang, S. B. Lee, E. J. Wiedenbrug, and M. R. Shah, "Automated detection of rotor faults for inverter-fed induction machines under standstill conditions," *IEEE Transactions on Industry Applications*, vol. 47, no. 1, pp. 55–64, 2011.

[8] M. F. Cabanas, F. Pedrayes, M. G. Melero, C. H. Rojas Garcia, J. M. Cano, G. A. Orcajo, and J. G. Norniella, "Unambiguous detection of broken bars in asynchronous motors by means of a flux measurement-based procedure," *IEEE Transactions on Instrumentation and Measurement*, vol. 60, no. 3, pp. 891–899, 2011.

[9] K. M. Sousa, I. Brutkowski Vieira da Costa, E. S. Maciel, J. E. Rocha, C. Martelli, and J. C. Cardozo da Silva, "Broken bar fault detection in induction motor by using optical fiber strain sensors," *IEEE Sensors Journal*, vol. 17, no. 12, pp. 3669–3676, 2017.

[10] B. D. Eddine Cherif, M. Bendjebbar, N. Benouzza, H. Boudinar, and A. Bendiabdellah, "A comparative study between two open-circuit fault detection and localization techniques in a threephase inverter fed induction motor," in *2016 8th International Conference on Modelling, Identification and Control (ICMIC)*, 2016, pp. 1–7.

[11] Z. Zhang, G. Luo, Z. Zhang, and X. Tao, "A hybrid diagnosis method for inverter open-circuit faults in pmsm drives," *CES Transactions on Electrical Machines and Systems*, vol. 4, no. 3, pp. 180–189, 2020.

[12] B. D. E. Cherif, M. Chouai, S. Seninete, and A. Bendiabdellah, "Machine-learning-based diagnosis of an inverter-fed induction motor," *IEEE Latin America Transactions*, vol. 20, no. 6, pp. 901–911, 2022.

[13] M. Z. Ali, M. N. S. K. Shabbir, S. M. K. Zaman, and X. Liang, "Single- and multi-fault diagnosis using machine learning for variable frequency drive-fed induction motors," *IEEE Transactions on Industry Applications*, vol. 56, no. 3, pp. 2324–2337, 2020.

[14] ——, "Machine learning based fault diagnosis for single-and multi-faults for induction motors fed by variable frequency drives," in *2019 IEEE Industry Applications Society Annual Meeting*, 2019, pp. 1–14.

[15] I. Martin-Diaz, D. Morinigo-Sotelo, O. Duque-Perez, and R. J. Romero-Troncoso, "An experimental comparative evaluation of machine learning techniques for motor fault diagnosis under various operating conditions," *IEEE Transactions on Industry Applications*, vol. 54, no. 3, pp. 2215–2224, 2018.

[16] H. S. Che, E. Levi, M. Jones, W.-P. Hew, and N. A. Rahim, "Current control methods for an asymmetrical six-phase induction motor drive," *IEEE Transactions on Power Electronics*, vol. 29, no. 1, pp. 407–417, 2014.

[17] J. E. T. Akinsola, "Supervised machine learning algorithms: Classification and comparison," *International Journal of Computer Trends and Technology (IJCTT)*, vol. 48, pp. 128 – 138, 06 2017.

Antonio Femia received the M.Sc. degree, with honors, in Electrical Engineering from the University of Bologna, Bologna, Italy, in 2021. Currently, he is pursuing a PhD in electrical engineering with the Department of Electric, Electronic and Information Engineering "G. Marconi", University of Bologna. His research fields include artificial intelligence applied to electric drives, diagnostic techniques for multiphase machines, and control strategies for power electronic converters.

Giacomo Sala (Member, IEEE) received the Ph. D. in Electrical Machines and Drives in 2018 from the University of Bologna, Italy. He worked as a researcher until 2019 in the Power Electronics, Machines and Control Group, Department of Electrical and Electronic Engineering, The University of Nottingham. Since 2019 he has been working as a researcher with the Department of Electrical, Electronic, and Information Engineering "Guglielmo Marconi" - DEI, University of Bologna, Italy, where he is currently employed as an Assistant Professor, since 2020. His research interests include design, modelling and control of multiphase electrical machines, fault tolerant controls and fault diagnosis of electric drives.
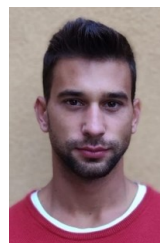
Luca Vancini received the M.Sc. degree in Electrical Engineering in 2018 from the University of Bologna, Bologna, Italy. Currently he is a postdoctoral fellow with the Department of Electric, Electronic and Information Engineering "G. Marconi", University of Bologna. His research interests include power electronics, control of multiphase converters and diagnostic techniques for multiphase machines.

Gabriele Rizzoli received the M.Sc and Ph.D. degree in Electrical Engineering respectively in 2012 and 2016, from the University of Bologna, Bologna, Italy. He is currently an Assistant Professor at the Department of Electrical, Electronic and Information Engineering "G. Marconi" of the University of Bologna. His research interests include the design of electrical machines, the development and control of high-efficient power converters for automotive and renewable energy applications.

Michele Mengoni (M'13) received the M.S. (with honors) and Ph.D. degrees in electrical engineering from the University of Bologna, Bologna, Italy, in 2006 and 2010, respectively. He is currently an Associate Professor with the Department of Electric, Electronic and Information Engineering "G. Marconi", University of Bologna. His research interests include design, analysis, and control of three phase electric machines, multiphase drives, and ac/ac matrix converters.

Luca Zarri (M'05-SM'12) was born in Bologna, Italy. He received the M. Sc. in Electrical Engineering, with honors, and the Ph.D. degree from the University of Bologna, Bologna, Italy, in 1998 and 2007, respectively. He worked as a freelance software programmer from 1989 to 1992 and as a plant designer with an engineering company from 1998 to 2002. In 2003 he became a laboratory engineer with the Department of Electric, Electronic and Information Engineering "G. Marconi", University of Bologna. He is currently a Full Professor of electric drives. He has authored or coauthored more than 170 scientific papers. His research activity concerns the control of power converters and electric drives. He is a senior member of the IEEE Industry Applications, IEEE Power Electronics and IEEE Industrial Electronics Societies.

Angelo Tani was born in Faenza, Italy, in 1963. He received the M. Sc. degree in Electrical Engineering, with honors, from the University of Bologna, Bologna, Italy, in 1988. Currently he is a Full Professor of power electronics, electrical machines and drives with the Department of Electrical, Electronic and Information Engineering "Guglielmo Marconi", University of Bologna. He has authored more than 200 papers published in technical journals and conference proceedings. His current activities include modelling, control and fault diagnosis of multiphase electric machines.